RSC Advances

ROYAL SOCIETY OF CHEMISTRY

www.rsc.org/advances

Light Trapping Effect in Plasmonic Blockade at the Interface of Fe_3O_4@Ag Core/Shell

Ahmad Yazdani[a]*, Mahdi Ghazanfari, Fatemeh Johar

Tarbiat Modares University, Jallal-Al-Ahmad Ave., Tehran, Iran, p.o.box 14115-111.

* Corresponding author: E-mail: yazdania@modares.ac.ir

Abstract:

The spherical isotropic magnetite (Fe_3O_4) nanoparticles were coated with a spherical isotropic Ag-shell in order to investigate the possibility of trapping photons through plasmon or plasmonic energy transfer enhancement at the magnetic-plasmonic interface coupling structure of core/shell. Our experimental results showed that: (1) The maximum broadening of optical absorption of Fe_3O_4 nanoparticles, as revealed by UV-Visible spectrophotometry, increases to a higher value due to the Ag shell thickness (7 nm), resulting in the decrease of saturation magnetization as measured with Vibrating Sample Magnetometer (VSM); (2) The measured saturation magnetization drops to a lower value as the maximum value of absorption shifts to a higher wavelength, because of the die out of two small peaks of Fe_3O_4 cited within 340-440 nm by the Ag plasmonic peak cited at 400 nm, which results in the shift; (3) The increased shouldering of absorption observed in UV-Visible spectrum decreases linearly by wavelength due to the increase of shell diameter, and ends to the initial maximum, which in turn results in the increase of saturation magnetization.

Introduction:

As it is known, Ag has a big negative real but a small positive imaginary permittivity. Half-ferromagnetic magnetite (Fe_3O_4) nanoparticles are so far the most commonly used magnetic carriers for a variety of biocompatible purposes. Despite the unique character of magnetite, the character of shell nanoparticles and its coupling with the magnetite core are questionable. There should be challenges on the core/shell "Fe_3O_4@Ag (or Au) [6-10] since the discover of the following;

(a) Surface Enhanced Raman Scattering (SERS) effect [11,12]

(b) Localized Surface Plasmon Resonance (LSPR), where collective oscillations of free conduction electrons in restricted curvature of metallic nanoparticles (MNPs) when illuminated with incident light cause strong optical responses at the plasmon resonance wavelength of MNPs as a non-propagating plasmon [13,14]. While the nanometer-range interaction between metal and semiconductor in core/shell nanoparticles when being light-illuminated causes to exhibit reinforced optical resonance and enhanced optical tunability in core/shell nanoparticles, which could be also a function of interface [15-17]. An effective approach for controlling and understanding the phenomena is as follows shell thickness, core diameter, electronic properties of shell and surrounding environment at two different interfaces (outer interface between the surface and incident light, and inner interface between metal and semiconductor), affect the plasmon resonance wavelength, light scattering, absorption and extinction cross section of core shell. LSPR causes some suitable characteristics such as enhancement of electric field, localization of energy at nanometer scale, and strongly enhanced absorption and scattering [18-20]. These characteristics make MNPs suitable candidates for various applications such as chemical and biological sensors [21] and enhanced spectroscopy devices.

Optical properties and enhanced optical-tunability of core shell nanoparticles (NPs) are determined by shape, size, permittivity, and geometrical arrangement of building blocks. The dependence of core shell NPs on geometry and electronic properties provide a keystone for designing core shell NPs with desired optical characteristics for various applications, such as solar cell optimization [22], near-infrared (NIR) photo-thermal imaging, photo-thermal therapy, electromagnetic interface shielding, and microwave absorption [23-25].

However, the properties of magnetite core particles such as reactivity, thermal stability, and magneto-optical properties could be investigated in order to achieve overall stability of particles and the dispersibility of core particles [26,27].

Since the decrease of the size of novel metals' nanostructures below the electron mean free path, gives rise to an intense absorption in the optical region associated with localized surface plasmon

resonance [28,29], the shell width and the geometry of the particle at the interface, which result in ratio of interior diameter of the shell and core diameter of the interface curvature, can be also more effective parameters. Whereas, the intimate contact with the core should strongly affect the phenomenon and is sensitive on the synthesis procedures.

Although various methods have been used to synthesis this material by controlling particle size, shape distribution, and geometrical formation [30,31], it has been discovered that the reduction, which is based on the decomposition and conversion of ethylene glycol to acetaldehyde [32], might be a convenient method for the growth of colloids on certain facets [33]. In this method, the temperature, which influences on the reduction potential of Polyol compound, leading to rupture and creation of chemical bonds and diffusion [34] and confined absorption at the surface of metal oxide, could be a dominant factor [34]. However, it has been reported that polyethylene glycol (PEG) with a uniform and ordered chain structure is easily absorbed at the surface of metal oxide colloids [35] and acts as a dispersion stabilizer. By using PEG as a surfactant, we could prevent the particle growth, decrease inter-particle interactions, and control the morphology.

In this paper, various reduction agent concentrations to deposit silver onto the magnetite Fe_3O_4 (which is a ferrimagnet with crystalline inverse cubic spinel structure, where magnetic moment of Fe^{+3} ions on A sites (tetrahedral site) are aligned anti-parallel to the magnetic moment of Fe^{+2} and Fe^{+3} on the B sites (octahedral site) with a metal insulator transition at 119 K [36]), was used to form a core/shell structure, in order to investigate the following;

(1) The effect of size on an aqueous ferro-fluid system, which contains spherical Fe_3O_4 nanoparticles coated with a spherical isotropic Ag-shell to develop an ideal interface contact to have a sufficient ratio of interior diameter of shell to the core diameter in the range of oscillation of conduction electron, in order to satisfy $P=\alpha E$.

(2) The closely-spaced Fe_3O_4@Ag nanoparticles, which are also a prerequisite for active SERS substrate.

(3) The confinement of conduction electron within a curved shape, on which the strength charge or/and consequently the LSPR density resulted to the induced optical pressure (P) to light trapping at the energy above the band gap play a big role [37-39]. Whereas it could be related to well-known fundamental electrostatic duo to the charge density induced (σ) on the surface when a metallic sphere is located in conductor cited in an electrical field as $P = 2\pi\sigma^2$.

Experimental:

Since pH could be an effective parameter as an electrostatic stabilizer to prevent the agglomeration during chemical reaction, sodium acetate was used to keep medium's pH relatively constant ~6.8. Chemical reagents used in this work were ferric chloride six hydrate ($FeCl_3 \cdot 6H_2O$), silver nitrate (AgNO3), sodium acetate, butylamine (99%), and polyethylene glycol (MW ~3000 Da). All reagents were of analytical grade purchased from Merck Co, and were used without further purifications.

Spherical-shaped magnetite nanoparticles were prepared following Deng et al. [40] and Kim et al. [41] method. In a typical method, $FeCl_3 \cdot 6H_2O$ (1.35 g, 5 mmol) was dissolved in ethylene glycol (40 mL) in an ultrasonic bath until a clear solution was formed. The pH of this solution was in the acidic range. After adding sodium acetate (3.7g, 45 mmol) and polyethylene glycol (1.0 g, 0.05 mmol) into the obtained solution, and vigorously stirring for 30 min, a homogeneous mixed was obtained. After being cooled to room temperature naturally, the black products were washed several times with ethanol and then dried at 80 °C for 8 h. In order to deposit silver onto the magnetite particles, first 4 mM ethanolic silvering solution was prepared. Next, 3 mg Fe_3O_4 nanoparticles were dispersed in 30 mL of this solution in a polypropylene container using an ultrasonic bath. The polypropylene container was used to avoid nonspecific silvering of the reaction vessel. Finally, silver coating was achieved by adding Butylamine as a weak reducing agent of AgNO3 in foregoing solution. The molar ratios of ethanolic silvering solution to Butylamine were varied as 1:0.5, 1:1, and 1:2, respectively. The yielded solution was incubated for 45 min at 50 ℃ in an ultrasonic bath.

After being rinsed with ethanol, the yielded product was redispersed in ethanol under sonication for 5 min.

Results and discussion:

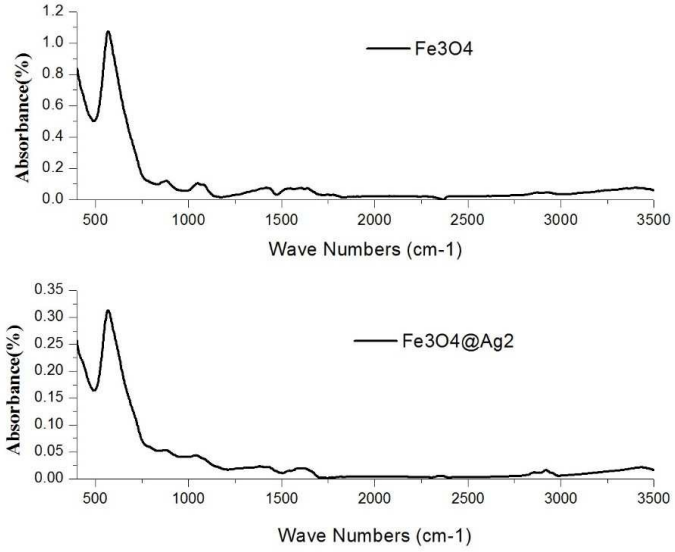

Fig. 1: FTIR spectra of Fe_3O_4 and Fe_3O_4@Ag1 core–shell nanospheres.

In order to investigate the strength of bond formation and the chemical impurities in the chemical process, the FTIR measurement was investigated, and the results are shown in Fig. 1. While there is no specific signal due to Ag because of its metallic nature, a strong absorption peak in both coated and pure magnetite ones located at 567 cm^{-1} is observable, which is attributed to the stretching vibration of Fe-O in tetrahedral sites. Some small band distributions, which are more obvious after the shielding probably due to restricted or/and the shell pressure at 1600 cm^{-1}, and the broad intense band observed within 3000–3500 cm^{-1} (with its maximum at 3400 cm^{-1}), are assigned to the bending of H-O-H molecules and the O-H stretching vibration, respectively. The peaks at 888 cm^{-1} and 1433 cm^{-1} are attributed to the rocking CH_3 and the bending -C-H vibrations, indicating the existence of polyethylene glycol. The crystal structure of Fe_3O_4 and the effect of shielding were studied by X-ray diffraction (XRD) pattern (see Fig. 2). The X-ray diffraction pattern of as-prepared magnetite was indexed in the Fd3m-Oh7 space group (no. 227) corresponding to a spinel cubic structure. After reduction of Ag ions, the resulting XRD pattern of the product was also investigated

in order to achieve a comparison between before and after reduction (see Fig. 2). After Ag was deposited on the surface of magnetite, four additional diffraction peaks were appeared at 2θ= 38.1, 44.3, 64.4, and 77.4° corresponding to (111), (200), (220), and (311) planes of silver, respectively, with a face-centered cubic (fcc) structure.

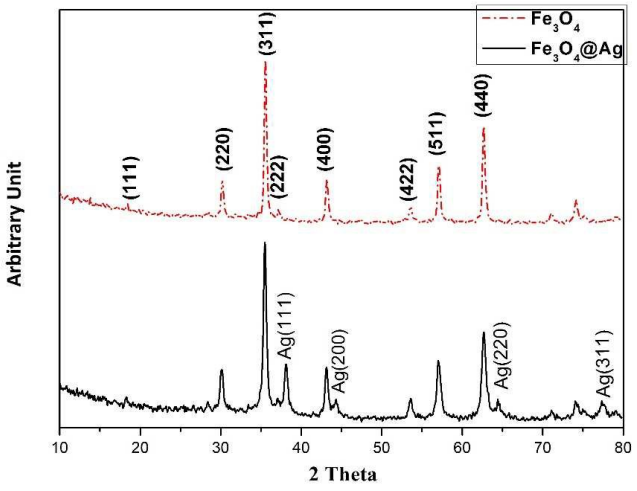

Fig. 2: X-ray diffraction patterns of Fe_3O_4 and Fe_3O_4@Ag1 core–shell nanospheres.

In addition to the calculation of lattice constants of the cubic crystal using d-spacing values and respective (hkl): (i) the average grain size was determined by applying Debye–Scherrer equation to the most intense peak; and (ii) the shape and distribution of the nanostructure, their homogeneity, and remarkable different morphologies were studied by both SEM and TEM, and the results are given in table 1.

Table1: Structural properties of Fe3O4 and Fe3O4@Ag core/shell nanoparticles.

Sample	Molar ratios of (ethanolic silvering solution: butylamine)	Lattice strain (%)	Lattice constant (nm)	Particle size (nm)
Fe_3O_4 NPs	--	0.385	0.838	14
Ag, sample 1	1:0.5	0.483	0.409	28
Ag, sample 2	1:1	0.474	0.408	28
Ag, sample 3	1:2	0.450	0.408	28

SEM micrograph shows clusters of fine particles sticking together and the aggregates have a spherical shape. The statistical histogram shows the mean diameter of Fe_3O_4 particles about 73 nm, as shown in Fig. 3(a). The formation of agglomerated clusters of particles is due to the magnetostatic coupling between the particles. The statistical histogram of the fine particles on the surface of the powders shows the primary particle size about 16 nm.

After reduction of Ag ions from the surface of magnetite, the smooth surface of yielded nanocomposites is clearly seen in Fig. 3 (SEM). The approximated thickness of silver shell is 7, 18, 22 nm for S1, S2, and S3, respectively.

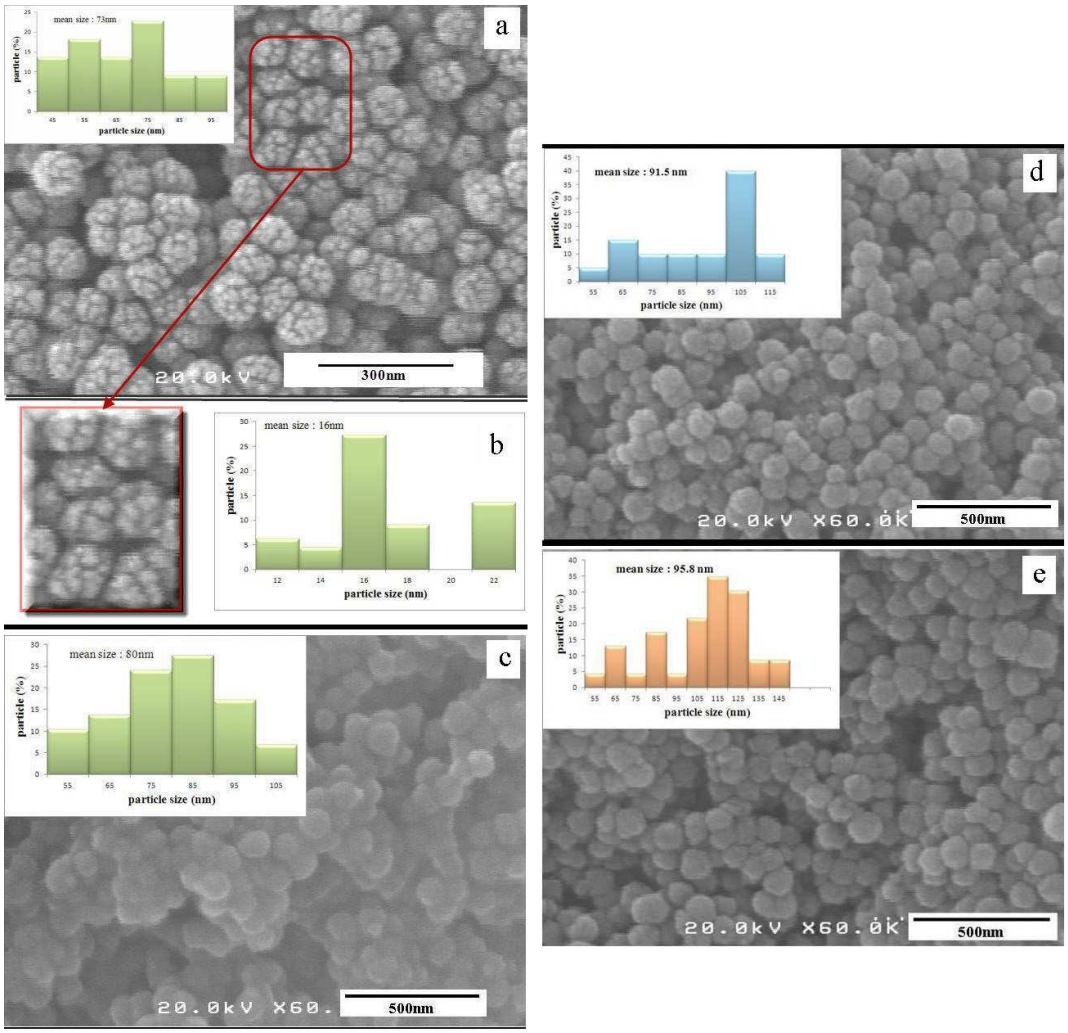

Fig. 3: (a) FESEM and statistical histogram images of as-prepared Fe_3O_4 nanoparticles synthesized by Polyol method; (b) fine particles on the surface of the powders ; (c) Fe_3O_4@Ag1, (d) Fe_3O_4@Ag2, (e) Fe_3O_4@Ag3.

Apart from the dependence on the nanoparticles' size and spherical distribution, it is evident that;

(1) It has not happened any nucleation of Ag in solution, and hence the reduction of silver has been shielded on the surface of Fe_3O_4.

(2) The closely-spaced formation of Ag shell on Fe_3O_4 nanoparticles was formed by the surface reaction controlled by the reduction of the surface-bond Ag, where TEM image shows a clear core/shell nanostructure. Although TEM image given in Fig. 4b shows various cores coated with Ag shell due to oxygen atoms on their surface, but the measured size is approximated close to the average size of (30, 41, 55 nm in Table 3).

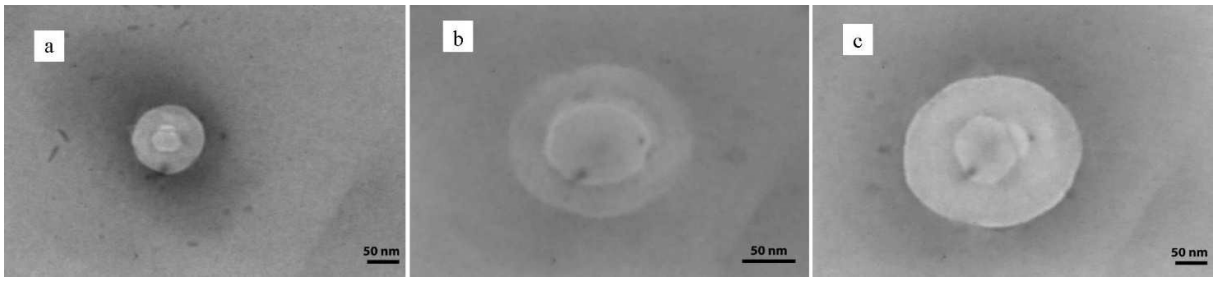

Fig.4: TEM images of (a) S1, (b) S2, (c) S3 Fe_3O_4@Ag nanoparticles.

To clear out the effect of interface coupling on the magnetic structure of the core, magnetic properties of the nanoparticles were characterized by VSM with a maximum applied field of 10 KOe. Fig. 5 shows the magnetic hysteresis loops of the nanoparticles at room temperature. Saturation magnetization (M_s), coercive field (H_c) and reduced remanent magnetization (M_r/M_s) are given in Table 2. The saturation magnetization value was 91 emu/gr for Fe_3O_4 that was the same as the value of bulk magnetite. It is easy to infer that the evolution behaviors of M_s and M_r are highly dependent on the growth of nanoparticles, because both the changes of M_s and M_r are associated with the average crystallite size, but here this high saturation magnetization may be attributed to the very thin dead layers observed in TEM. The reduced remanent magnetization (the ratio of the remanence (M_r) to the saturation magnetization (M_s)) shows the value expected for random assemblies of single-domain nanoparticles with magnetostatic coupling. By using polyethylene glycol as a surfactant to separate and restrict the growth of the particles, magnetostatic interactions

are dominated in agreement with the remanence ratio analysis. The saturation magnetization decreased as the molar ratio of Butylamine increased. It corresponds to the increased diamagnetic silver nanoparticles distributed on the surface of magnetite. The coercivity of the magnetite and the Fe_3O_4@Ag core/shell nanoparticles were ~50 Oe. The Ag shell was appeared to have no significant effect on the coercivity of the magnetite.

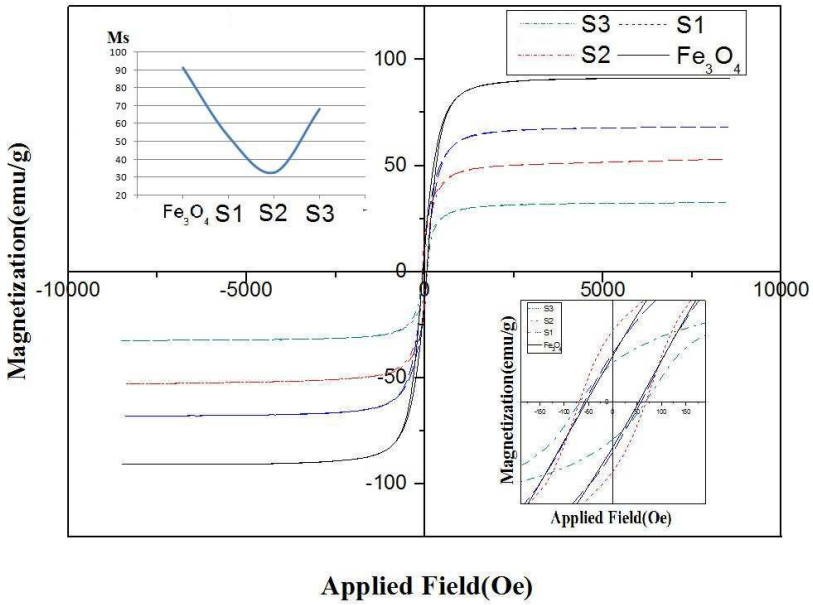

Fig. 4: Magnetization curve of Fe_3O_4 and Fe_3O_4@Ag core–shell nanospheres at room temperature. Inset a shows a hysteresis like loop. Inset b shows the variation of saturation.

Table 2. Saturation magnetization values for different samples.

Samples	**Saturation magnetization (emu/g)**	**Coercivity (Oe)**	**M_r (emu/gr)**	**M_r/M_s**
Fe_3O_4 NPs	91.283	53	11	0.12
Fe_3O_4@Ag, sample 1	53.062	68	17	0.33
Fe_3O_4@Ag, sample 2	32.596	67	9	0.29
Fe_3O_4@Ag, sample 3	68.231	57	11	0.17

Consequently, the interface matching of core/shell is indicated as a better approximation related to the geometrical parameters of shape, size, and curvature of nanoparticles. This leads to the response character of opto-magnetic behavior of Fe_3O_4 and its core/shell Fe_3O_4@Ag, which is evident in the characteristic behavior of UV-visible absorption spectrum (Fig. 6) resulted to saturation magnetization on which both are attributed to the diameter of shell boundary Fig. 5. Whereas it is evident that the characteristic behavior of UV-visible absorption spectra of Fe_3O_4 (Fig. 6a) changes as it is treated with the silvering medium Fig. 6 (b, c, d) as the following observations (which is in agreement with the reported result elsewhere [42,43]), which leads to the magnetization structure specially saturation magnetization, which is attributed to the shell thickness.

1) A broad maximum absorption around 500 nm in the UV-visible spectra for Fe_3O_4 nanoparticles, below which a small peak cited within 340-440 nm is more pronounced before the shielding, where the measured saturation magnetization is about 91 emu/gr.,

2) Upon the deposition of silver, not only the broad maximum distribution of characteristic Fe_3O_4 is increased, but also the noticeable small cited maximum peak within 340-440 nm (Fig. 7a) is suppressed with the maximum absorbing peak of Ag cited at 400 nm (Fig. 7b). This suppression of two peaks is vanished in direction to shift the intrinsic maximum absorption (at 500 nm) to a higher wavelength. In order to reveal the cause of this observation, the UV-visible absorption of Ag nanoparticle synthesized by arc-melt in liquid was also studied. The absorption peak of colloidal dispersion of prepared Ag nanoparticles having sizes in the range (8-13 nm) is at ~400 nm similar to the other works [44-46] (see Fig. 7b). This maximum may also be lowered to the two maximum noticeable distribution peaks, which is reported on core/shell Fe_3O_4/Ag and Fe@Fe_3O_4 (Fig. 7b) [42,43]. The vanishing of both, the damping maximum Ag to two peaks of Fe_3O_4 is strongly eliminated upon the drop of saturation magnetization from 91 emu/gr to 38-48 emu/gr. The phenomenon is a consequence of the limited width of coupling interface between novel metallic Ag shell and semiconducting magnetite Fe_3O_4 core, which was measured using SEM and TEM images about ~7 nm upon the deposition of silver on the as-synthesized sample.

3) The maximum value of broadening absorption for the sample S1 decreases linearly to its maximum originated from Fe_3O_4 as the shell diameter increases table.3 (see Fig. 6 inset). This phenomenon is assumed to be due to the characteristic behavior of Fe_3O_4 and decoupling of Ag nanoparticles, in which the vanished maximum distribution peak is regenerated with a small shift, where the saturation magnetization is also increased. However, in every cases, the estimation of the type of optical transition across the band gap of Fe_3O_4 semiconductor is difficult. The band gap is reported within 0-3 eV [46] and high different values 5-1.9 and also 0.1 eV [47-49], while in our case it is estimated to be about 1.8-1.4 which is determined by the well-known Tauc's relation (see Table.3, Fig. 7)

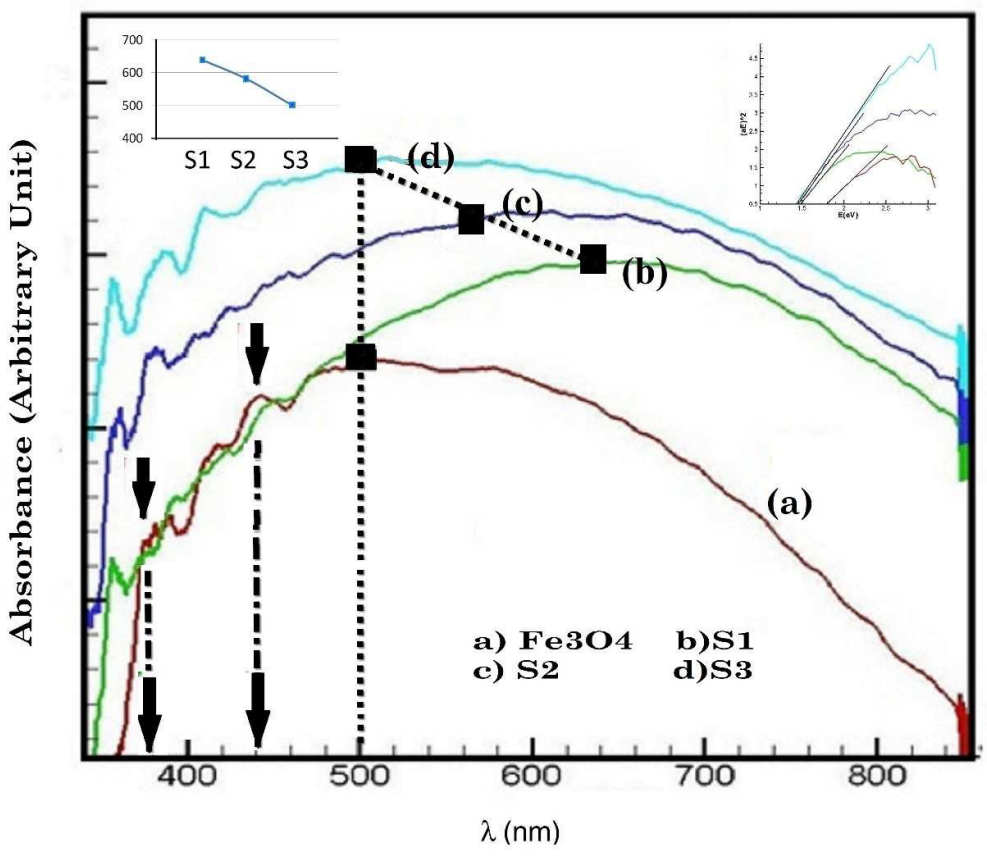

Fig. 6: UV-Vis spectra of NPs. Inset shows the estimation of band gap by Tuac's relation. The region indicated by an arrow in Fig. 6, is same as that studied in Fig. 7.

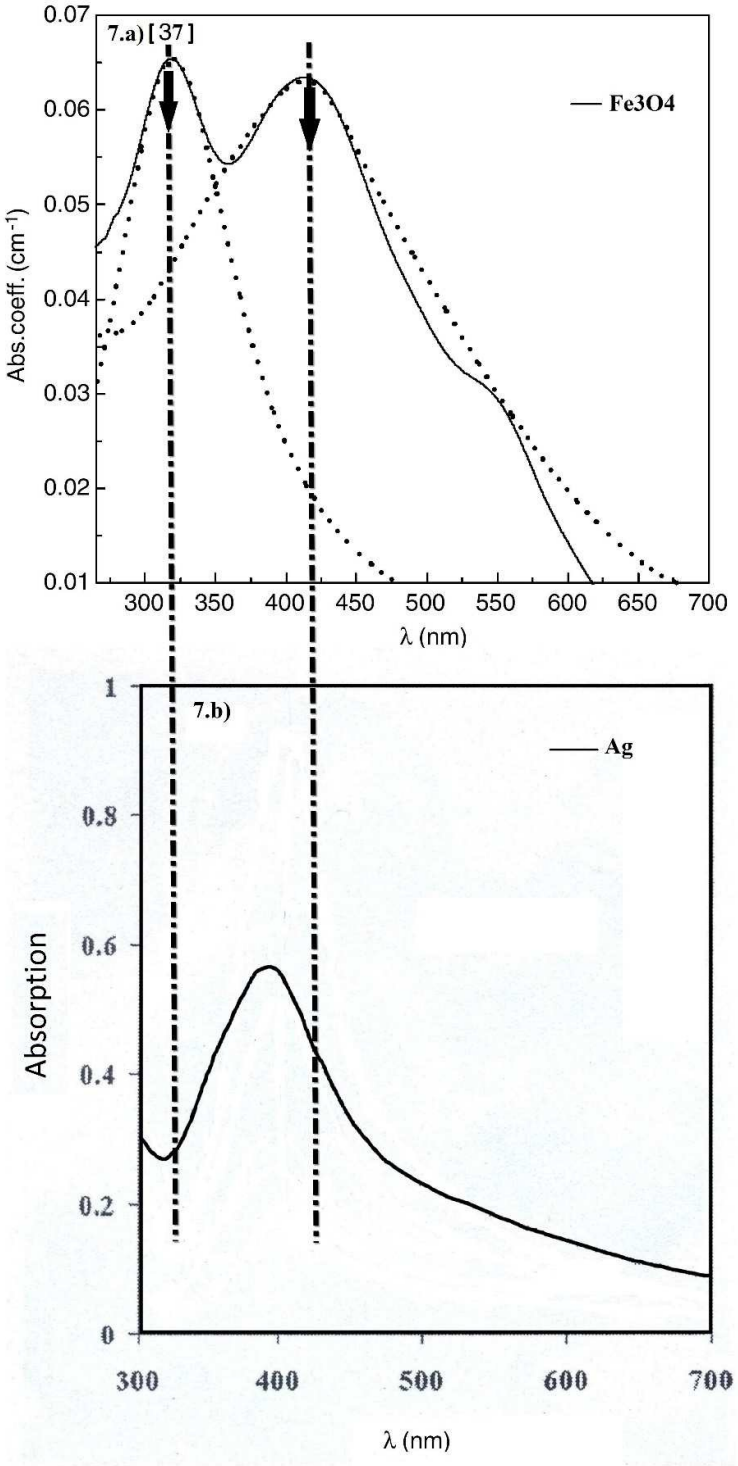

Fig. 7: (a) Comparison of experimental optical analyze with theoretical fit for magnetite nanoparticles"Fe_3O_4" to clear out the intrinsic optical absorption in the wave length within 334-440 nm [40]. (b) Optical absorption of silver nanoparticle prepared with the arc melt fullness in water.

Table 3. The UV-visible values for different samples.

sample	Peak (nm)	Eg(eV)	Core (nm)	Shell (nm)	
Fe_3O_4	500	1.8		**TEM**	**SEM**
S1	640	1.48	50	30	7
S2	580	1.46	85	41	18
S3	500	1.44	90	55	22

However, although the intense absorption region in UV-visible spectrum to the red shift could be attributed to the resonant behavior of LSPR, which is originated from the confined conduction electron within the geometrical core/shell curvature, it could also be a consequence of the following:

(i) The dielectric relation function $E_m = E_0 F(\frac{\varepsilon_{Ag}}{\varepsilon_{Fe_3O_4}})$ that results in a tunable restricted interface;

(ii) The dependence strength of coupling interface on the density of conduction electron, which lead to an electron mean free path equal to the size of nanoparticles' interface [50-52]. However, the plasmonic coupling between deposited Ag nanoparticles and the interface structure between the Ag and Fe_3O_4 of hybrid particles may also be the cause [53-55];

(iii) The increased absorbance within 400-500 nm is presumed to be due to the Mie plasmon resonance excitation from the silver nanoparticles.

However, the strong evident absorption of sample S1, which results in the drop of saturation magnetization from 91 emu/gr to 38-48 emu/gr can be a consequence of the following;

(a) Both induced optical pressure of "conduction electron" and charge and plasmonic transfer;

(b) Photon-generated electrons in the depth of coupling of Fe_3O_4 enclosed to Ag shell, which may due to the excited photo-threshold of Fe^{+3} to Fe^{+2} by transferring the energy contained in the oscillating electrons or local plasmonic field from the metal to the magnetite via (i) direct electron transfer and/or (ii) plasmon-induced resonant energy transfer;

(c) Since, the interface matching of core/shell is sensitive to the ratio of particle size to the optical absorption depth, the charge-induced polarization "P=αE" and the consequence of being a functional of the dielectric relation $E_m = E_0 F(\frac{\varepsilon_{Ag}}{\varepsilon_{Fe_3O_4}})$, could effectively depend on the contact shell diameter, where a strong evident absorption is observed and the optical depth is about ~7 nm that resulted to the dropped magnetization;

(d) Consequently, the induced optical pressure, defined by the strength of density of charge and plasmon on the surface curvature, which could be related to the well-known fundamental electrostatic phenomenon when a metallic sphere is located in the electric filed $P=4\pi\sigma^2$,where P is the electrostatic pressure due to the surface charge density of 'σ'.

Conclusion:

Consequently, by forming silver shell on magnetite, the red shift is observed. This observation could be attributed to the LSPR-induced charge separation, by transferring the energy contained in the oscillating electrons or local plasmonic field from the metal to the magnetite via (i) direct electron transfer and/or (ii) plasmon-induced resonant energy transfer. This is referred to as plasmonic energy transfer enhancement and is stronger in small metal nanoparticles with small scattering cross-sections [56]. By increasing shell thickness, the incident light is efficiently scattered multiple times, increasing the optical path length and the light absorption in magnetite core, which is referred to as light trapping which contributes to enhancement at the energies above the band gap of a magnetite [57,58].

The energy absorbed by LSPR could be transferred to Fe_3O_4 semiconductor, which may be a consequence of the die out of distribution of small maximum peak below the intrinsic broad maximum value (at ~500 nm) by maximum absorption of Plasmon observed at ~400 nm for Ag nanoparticles resulted to;

(1) The decrease of saturation magnetization to a lower value;

(2) The shift of maximum absorption value of Fe_3O_4 to a higher value for the first sample with the Ag shell thickness of ~7 nm;

(3) As the shell thickness increases (S2 and S3 samples with thicknesses of 18 and 22 nm, respectively), the maximum absorption value decreases linearly to its initial value, which may be attributed to the plasmon-induced resonance energy transfer as well as the optical pressure-induced charge transfer to the Fe_3O_4 above bandgap, below which the increased absorbance within 400-500 nm is assumed to be due to the Mie Plasmon resonance excitation from silver nanoparticles.

These results could provide a general approach to overcome the low optical absorption in the broad range band and make it possible to exploit more percent of solar energy, as well as make them a better photocatalyst under solar light.

References:

[1] F. Sauzedde, A. Elaissari, C. Pichot, Colloid and Polymer Science, 1999, 277, 846.

[2] P.K. Jain, X.Yanhong, W. Ronald, E.C. Adam, Nano letters, 2009, 9(4), 1644.

[3] C.F. Bohren, D.R. Huffman, Absorption and scattering of light by small particles, (Wiley-Vch, 2008).

[4] K. Saha, S. A. Sarit, K. Chaekyu , L. Xiaoning , M.R. Vincent, Chemical reviews, 2012, 112(5), 2739.

[5] X. Huang, P.K. Jain, IH. El-Sayed, MA. El-Sayed, Lasers in medical science, 2008, 23(3), 217.

[6] Y. Cui, D. Hu, Y. Fang, J. MA, Science in China (Series B), 2001, 44, 404.

[7] U. Häfeli, Scientific and Clinical Applications of Magnetic Carriers, 1997, 1.

[8] M. Mandal, S. Kundu, S.K. Ghosh, S. Panigrahi, T.K. Sau, S.M. Yusuf, T. Pal, J. Colloid Interface Science, 2005, 286,187.

[9] D. H. Zhang, G.D. Li, J.X. Li, J.S. Chen, Chemical Communications, 2008, 29, 3414.

[10] G. Bhargava, I. Gouzman, C.M. Chun, T.A. Ramanarayanan, S.L. Bernasek, Applied Surface Science, 2007, 253, 4322.

[11] J. Du, C. Jing, Journal of Colloid and Interface Science, 2011, 358, 54.

[12] K. Kim, H. Ryoo, K.S. Shin, Langmuir, 2010, 26, 10827.

[13] K. L. Kelly, E. Coronado, L. Zhao, and G. C. Schatz, Journal of Physical Chemistry B, 2003, 107, 668.

[14] P. K. Jain, K. S .Lee, I. H. El-Sayed, M. A. El-Sayed, Journal of Physical Chemistry B, 2006,110, 7238.

[15] T. W. Ebbesen, C. Genet, S. I. Bozhevolnyi, Physics Today, 2008, 61(5), 44.

[16] L. Novotny, Physics Today, 2011, 64 (2), 47.

[17] M. I. Stockman, Physics Today, 2011, 64(2), 39.

[18] S. A. Maier, Plasmonics: Fundamentals and Applications, (New York: Spinger -Verlag, 2007).

[19] M. Pelton, J. Aizpurua, G. Bryant, Laser and Photonics Reviews, 2008, 2, 1.

[20] V. Giannini, I. Fernández-Domínguez, Y. Sonnefraud, T. Roschuk, R. Fernández-García, S.A. Maier, Small, 2010, 6, 2498.

[21] G. A. Sotiriou, S. E. Pratsinis, Current opinion in Chemical Engineering, 2011, 1, 3.

[22] K. Nakayama, K. Tanabe, H.A. Atwater1, Applied Physics Letter, 2008, 93, 121904.

[23] Z. Guo, S. Park, H.T. Hahn, S. Wei, M. Moldovan, A.B. Karki, D.P. Young, Journal of Applied Physics, 2007, 101, 09M511.

[24] Z. Guo, S. E. Lee, H. Kim,S. Park, H.T. Hahn, A.B. Karki, D.P. Young , Acta Materialia, 2009, 57, 267.

[25] S. W. Phang, N. Kuramoto, Polymer Composites, 2010, 31, 516.

[26] J. Wan, W. Cai, X. Meng , E. Liu, Chemical Communications, 2007, 47,5004.

[27] P.K.Jain, Y. Xiao, R. Walsworth, A.E. Cohen, Nano letters, 2009, 9(4),1644.

[28] A. H. Atwater, A. Polman, Nature Material, 2010, 9, 205.

[29] S. Warren, E. Thimsen, Energy and Environmental Science, 2012, 5, 5133.

[30] W.Cai, J. Wan, Journal of Colloid and Interface Science, 2007. 305(2), 366.

[31] S. W. Cao, Y. J. Zhu, and J. Chang, New Journal of Chemistry, 2008. 32(9), 1526.

[32] N.L. Drake, T.B. Smith, Journal of the American Chemical Society, 1930, 52(11), 4558.

[33] M. Bognitzki, H. Hou, M. Ishaque, T. Frese, M. Hellwig, C. Schwarte, A. Schaper, J. H. Wendorff , A. Greiner, Advanced Materials, 2000. 12(9), 637.

[34] T. Ding, H. Wang, S. Xu, J. Zhu, Journal of crystal growth, 2002, 235(1), 517.

[35] J. Dobryszycki, S. Biallozor, Corrosion Science, 2001, 43(7), 1309.

[36] E. J. W. Verwey, P.W. Haayman, Physica, 1941, 8, 979.

[37] V.E. Ferry, J. N. Munday, H. A. Atwater, Advanced Materials, 2010, 22, 4794-4808.

[38] E. Thimsen, F. Formal, M. Gratzel, S. Warren, Nano Letters, 2011, 11, 35-43.

[39] K. Aydin, V. E. Ferry, R. M. Briggs, H. A. Atwater, Nature Communications, 2011, 2, 517.

[40] H. Deng, X. Li, Q. Peng, X. Wang, J. Chen , Y. Li, Angewandte Chemiestry, 2005. 117(18), 2842.

[41] E. H. Kim, H. S. Lee, B. K. Kwakb, B.-K. Kim, Journal of Magnetism and Magnetic Materials, 2005. 289(0), 328-330.

[42] K. Kim, J.Y. Choi, H.B. Lee, K.S. Shin, ACS Applied Materials & Interfaces, 2010, 2(7), 1872.

[43] S. Basu, D. Chakravorty, Journal of non-Crystalline Solids, 2006, 352, 380.

[44] A.V. Hoonacker, P. Englebienne, Current Nanoscience, 2006, 2, 359.

[45] A.A. Ashkarran, A. Iraji zad, M.M. Ahadian, M.R. Hormozi Nezhad, The European Physical Journal Applied Physics, 2009, 48, 10601.

[46] W. H. Strehlow and E. L. Cook, Journal of Physical Chemistry, 1973, 2, 1.

[47] R. S. Gaikwad, S.Y. Chae, R.S. Mane, S.H. Han, O.S. Joo, International Journal of Electrochemistry, 1973, 2, 1.

[48] H.El Ghandoor, H. M. Zidan Mostafa M.H. Khalil, M. I. M. Ismail, International Journal of Electrochemistry Science, 2012, 7, 5734.

[49] Y. Tian, D. Wu, X. Jia, B. Yu, S. Zhan, Journal of nanomaterials, 2011, 2011, Article ID 837123, 5 pages.

[50] W. Wu, Q. He, H. Chen, J. Tang, L. Nie, Nanothecnology, 2007, 18, 145609.

[51] J. B. Jackson, S. C. Westcott, L. R. Hirsch, J. L. West, N. Halas, Journal of Applied Physics Letters, 2003, 82, 257.

[52] X. Xia, Y. Liu, V. Backman, G. A. Ameer, Nanothecnology, 2006, 17, 5435.

[53] H. Dotan, O. Kfir, E. Sharlin, O. Blank, M. Gross, I. Dumchin G. Ankonina, A. Rothschild, Nature Materials, 2013, 12, 158-164.

[54] S. K. Cushing, N. Wu, The Electrochemical Society Interface, 2013, 22, 63-67.

[55] S. K. Cushing, J. Li, F. Meng, T. R. Senty, S. Suri, M. Zhi, M. Li, A. D. Bristow, N. Wu, Journal of The American Chemical Society, 2012, 134, 15033-15041.

[56] J. Li, S. K. Cushing, P. Zheng, F.E. Meng, D. Chu, N. Wu. Nature communications. 2013, 4, 2651.

[57] V. E. Ferry, M. A. Verschuuren, H. B. T. Li, E. Verhagen, R. J. Walters, R. E. I. Schropp, H. A. Atwater, A.Polman, Optics Express, 2010, 18(102), A237-A245.

[58] V. E. Ferry, M. A. Verschuuren, M. C. Lare, R. E. I. Schropp, H. A. Atwater, A. Polman. Nano Letters, 2011, 11(10), 4239-4245.